Supporting Information

Comparative Study on the Photovoltaic Characteristics of A–D–A and D–A–D Molecules Based on Zn-Porphyrin; a D–A–D Molecule with Over 8.0% Efficiency

Virginia Cuesta, Maida Vartanian, Pilar de la Cruz, Rahul Singhal, Ganesh D. Sharma and Fernando Langa**

1. Experimental conditions

All solvents and reagents were purchased from Aldrich Chemicals. The solvents were used without previous purification, except $CHCl_3$ that was filtrated over neutral alumina for the synthesis of **5** and **8**. Anhydrous solvents were dried by purification system Pure-Sov 400. Chromatographic purifications were performed using silica gel 60 Merk 230-400 mesh ASTM. Gel Permeation Chromatograpy (GPC) column was performed using Bio-Beads ® S-X1 Beads 200-400 Mesh as stationary phase. Analytical thin-layer chromatography was performed using ALUGRAM ® SIL G/UV_{254} silica gel 60. Nuclear magnetic resonance ^{1}H NMR and ^{13}C NMR were performed using Bruker Innova 400 Hz, except the spectra ^{1}H NMR and ^{13}C NMR of **1** and **2** which were performed using Bruker AVIII 700 MHz at 50°C. Chemical shifts (*δ)* values are denoted in ppm. Residual solvent peaks being used as the internal standard ($CHCl_3$, δ = 7.27 ppm). ^{13}C NMR chemical shifts are reported relative to the solvent residual peaks ($CDCl_3$, δ = 77.00 ppm). MALDI-TOF spectra were obtained in VOYAGER DETM STR spectrometry, using dithranol [1,8-dihydroxy-9(10H)-anthracenone] as matrix. Fourier transform infrared spectrophotometer (FT-IR) Thermo Nicolet AVATAR 370 was used with ATR (Attenuated Total Reflection) method, in each case the most characteristic bands are indicated for each compound. Absorption spectra were performed on Shimadzu UV 3600 spectrophotometer. Solutions of different concentration were prepared in CH_2Cl_2, spectroscopy grade, with absorbance between 0.2 and 0.3 using a 1 cm UV cuvette. Film thickness for UV-Vis were deposited by spin-coating (60 s, 3000 rpm) on cover slips (22x22 mm) from solutions of **1** and **2** in $CHCl_3$. The thermal stability was evaluated by TGA on a Mettler Toledo TGA/DSC Start^{e} System under nitrogen, with a heating rate of 10 °C/min.

Electrochemical Measurements: Reduction (E_{red}) and oxidation potentials (E_{ox}) were measured by cyclic voltammetry with a potentiostat BAS CV50W in a conventional three-electrode cell equipped with a glassy carbon working electrode, a platinum wire counter electrode, and an $Ag/AgNO_3$ reference electrode at scan rate of 100 mV/s. The E_{red} and E_{ox} were expressed vs. Fc/Fc^{+} used as external reference. In each case, the measurements were done in a deaerated solution containing 1

mM of a the sample compound in 0.1 M of $(n\text{-Bu})_4NClO_4$ in *o*-DCB:Acetonitrile (4:1) as an electrolyte solution.

Computational Details: Theoretical calculations were carried out within the density functional theory (DFT) framework by using the Gaussian 09, applying density functional theory at the B3LYP level. The basis set of 6-31G* was used in the calculations (Supercomputation Service of UCLM).

Device fabrication and characterization: All the organic solar cells were fabricated using conventional structure i.e. ITO/PEDOT/active layer/PFN/Al. First of all, patterned indium tin oxide (ITO) coated glass substrates were cleaned via ultrasounds in deionized water, acetone and iso-propanol sequentially for 10 min each and dried in ambient conditions to remove the residuals. Then they were coated with PEDOT:PSS (~35 nm) and dried at 120 °C for 10 min. After that the active layers of **1** or **2**:$PC_{71}BM$ (in different weight ratios) were spin coated on the top of PEDOT:PSS layer from chlorobenzene solution at a total concentration of 16 mg/ml and dried at 50°C in vacuum oven for 20 min to remove the residual. A thin layer of PFN was spin coated on the top of active layer, which was dissolved in methanol and mixed with acetic acid with a concentration of 0.5 mg/ml and then spin coated at rpm of 2000 to get a thin film of about 10 nm. Finally, aluminium (Al) was thermally evaporated on the top of PFN to make the device. The current–voltage measurements were carried out in the dark as well as under a simulated 1.5G light source with an intensity of 100 mW/cm^2 using a xenon-lamp-based solar simulator and data were collected with a computer-controlled Keithley 2400 Source Measure Unit.

The incident photon to current efficiency (IPCE) of the devices was measured illuminating the device through the light source and monochromators and the resulting current was measured using a Keithley electrometer under short circuit conditions. The hole-only and electron only devices with ITO/PEDOT:PSS/active layer/Au and glass/Al/active layer/Al, respectively were also fabricated in an analogous way, in order to measure the hole and electron mobilities.

^{1}H NMR, ^{13}C NMR, FT-IR and MALDI-TOF MS spectra

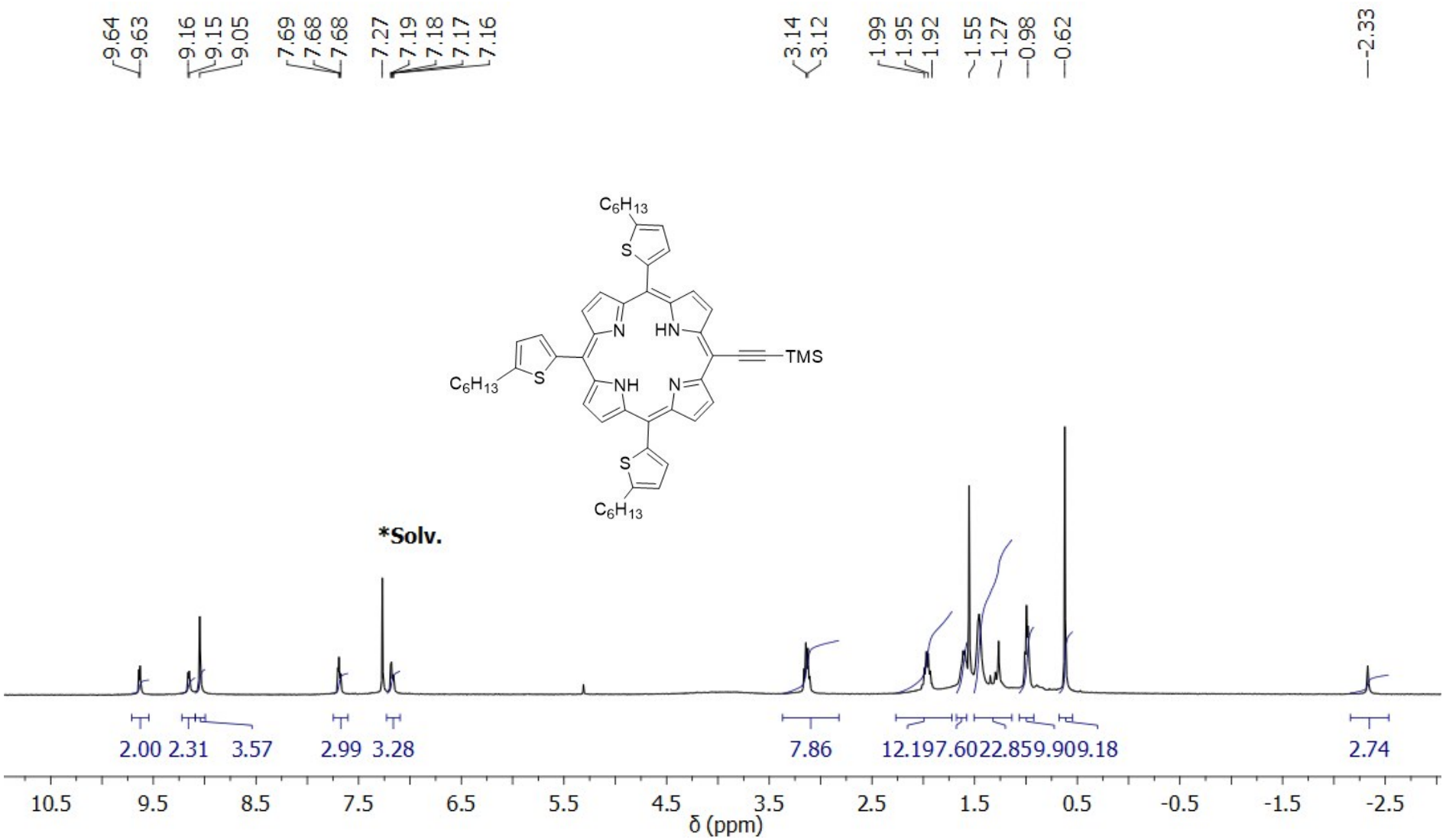

Figure S1. ^{1}H NMR spectrum of **A_3B-H_2** (400 MHz, $CDCl_3$).

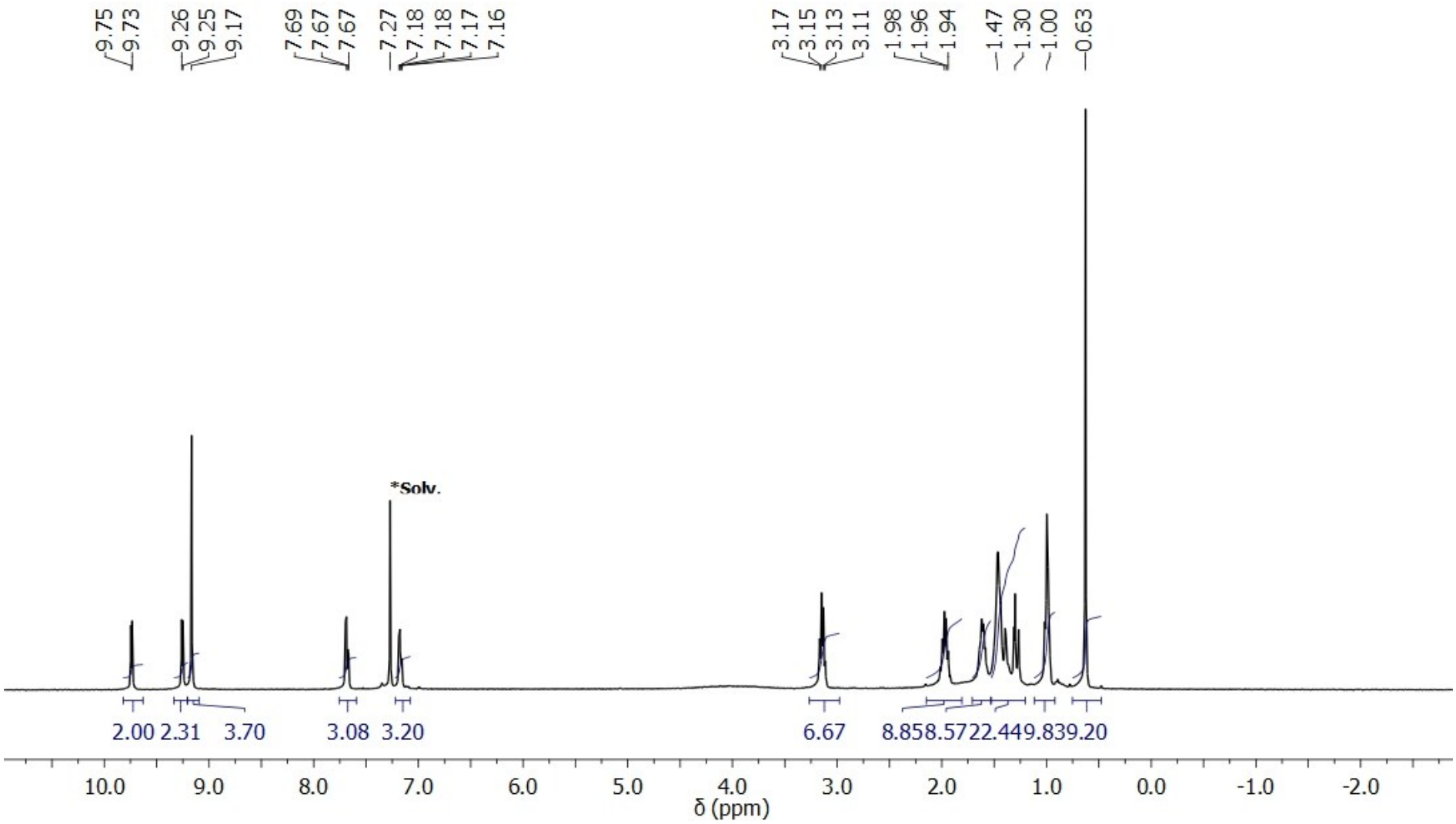

Figure S2. ^{1}H NMR spectrum of **6** (400 MHz, $CDCl_3$).

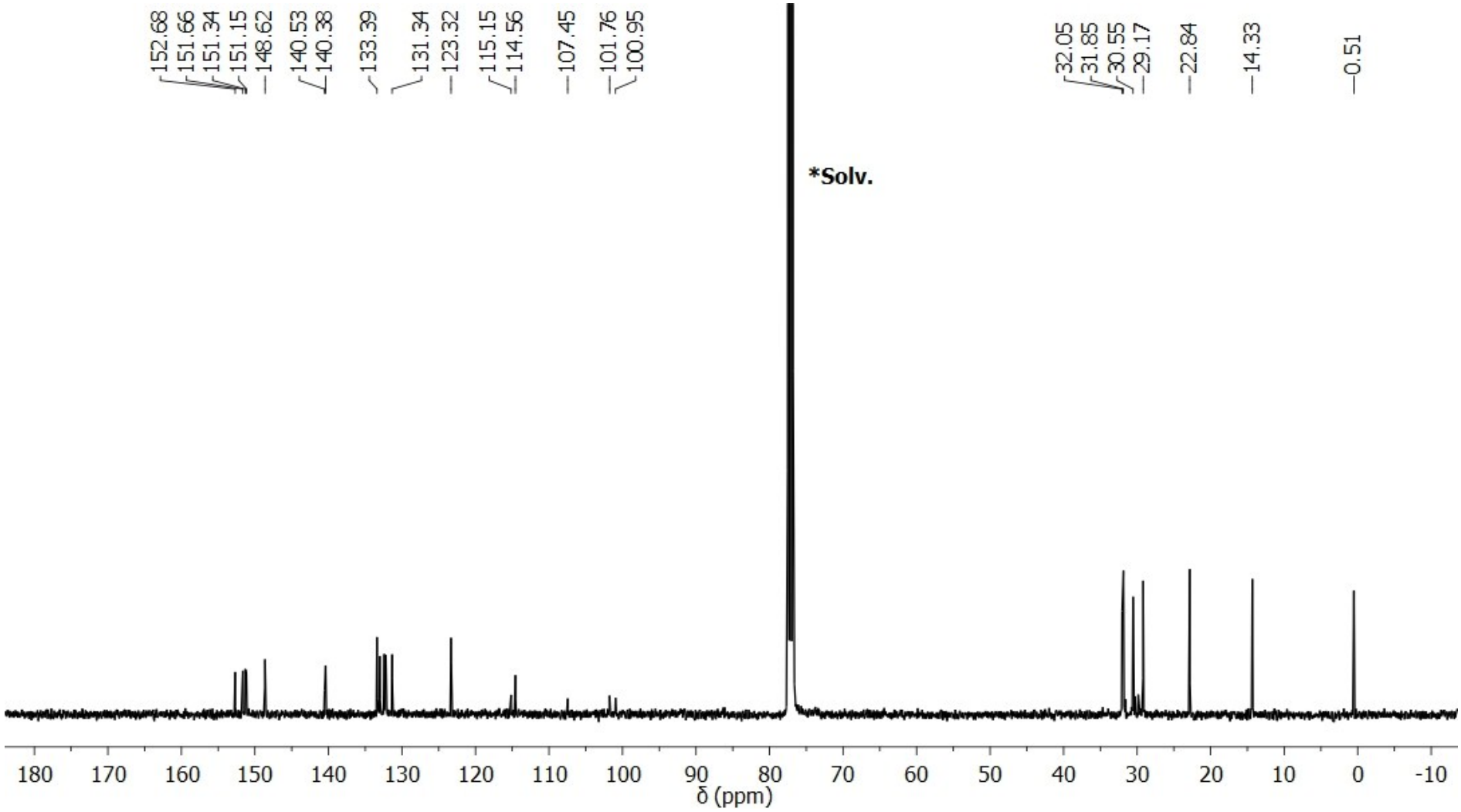

Figure S3. ^{13}C NMR spectrum of **6** (100 MHz, $CDCl_3$).

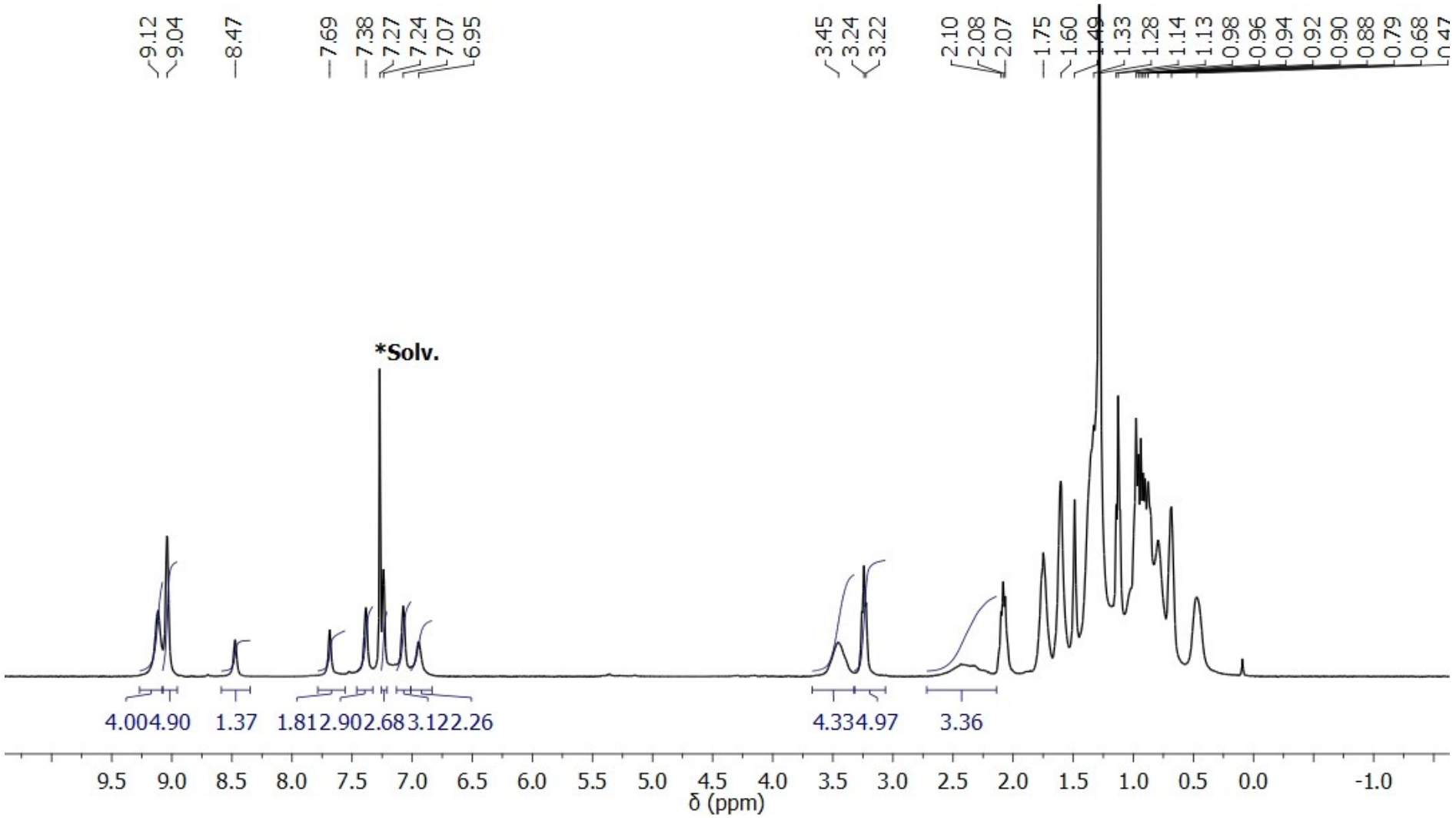

Figure S4. ^{1}H NMR spectrum of **1** (700 MHz, $CDCl_3$, 50 °C).

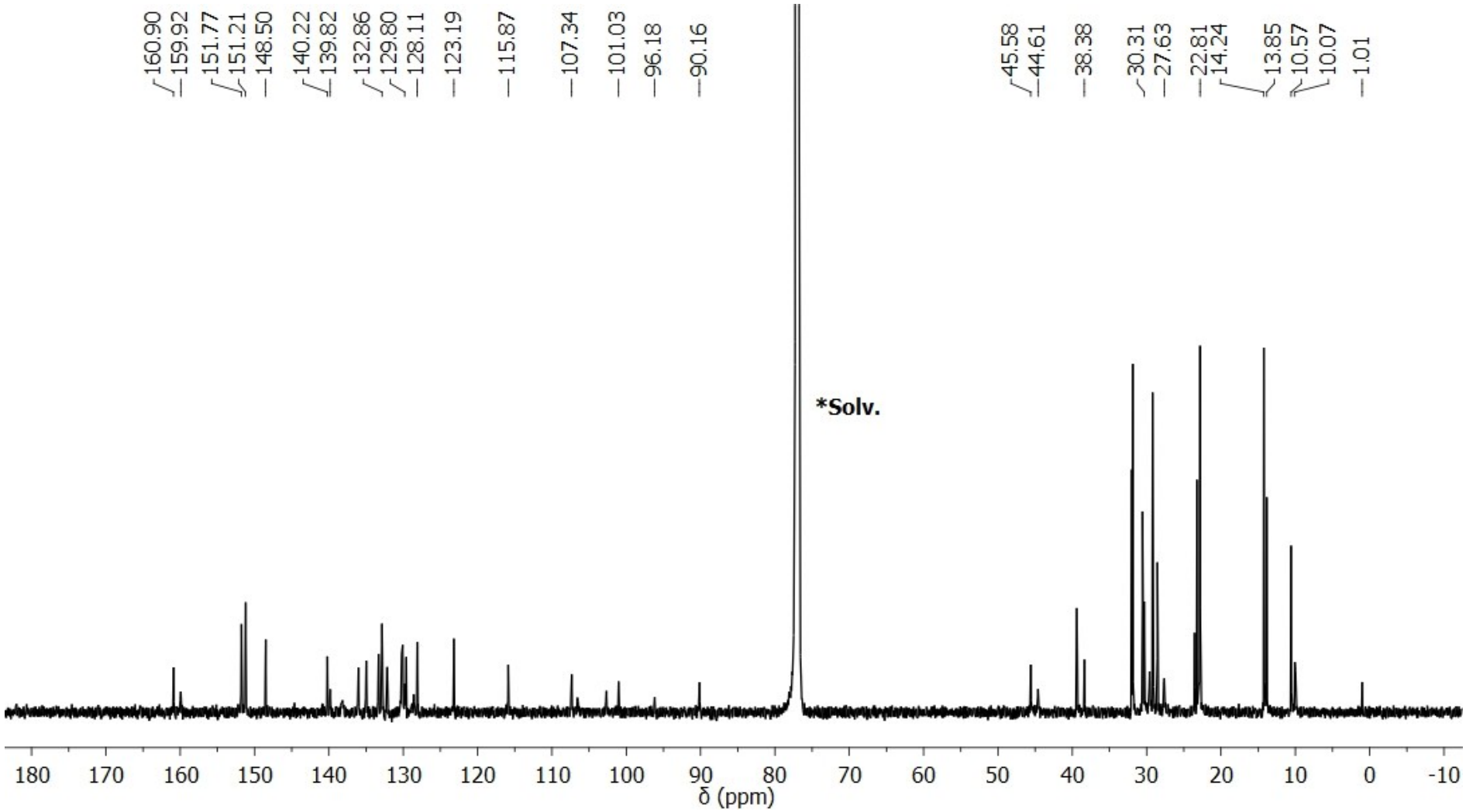

Figure S5. ^{13}C NMR spectrum of **1** (175 MHz, $CDCl_3$, 50 °C).

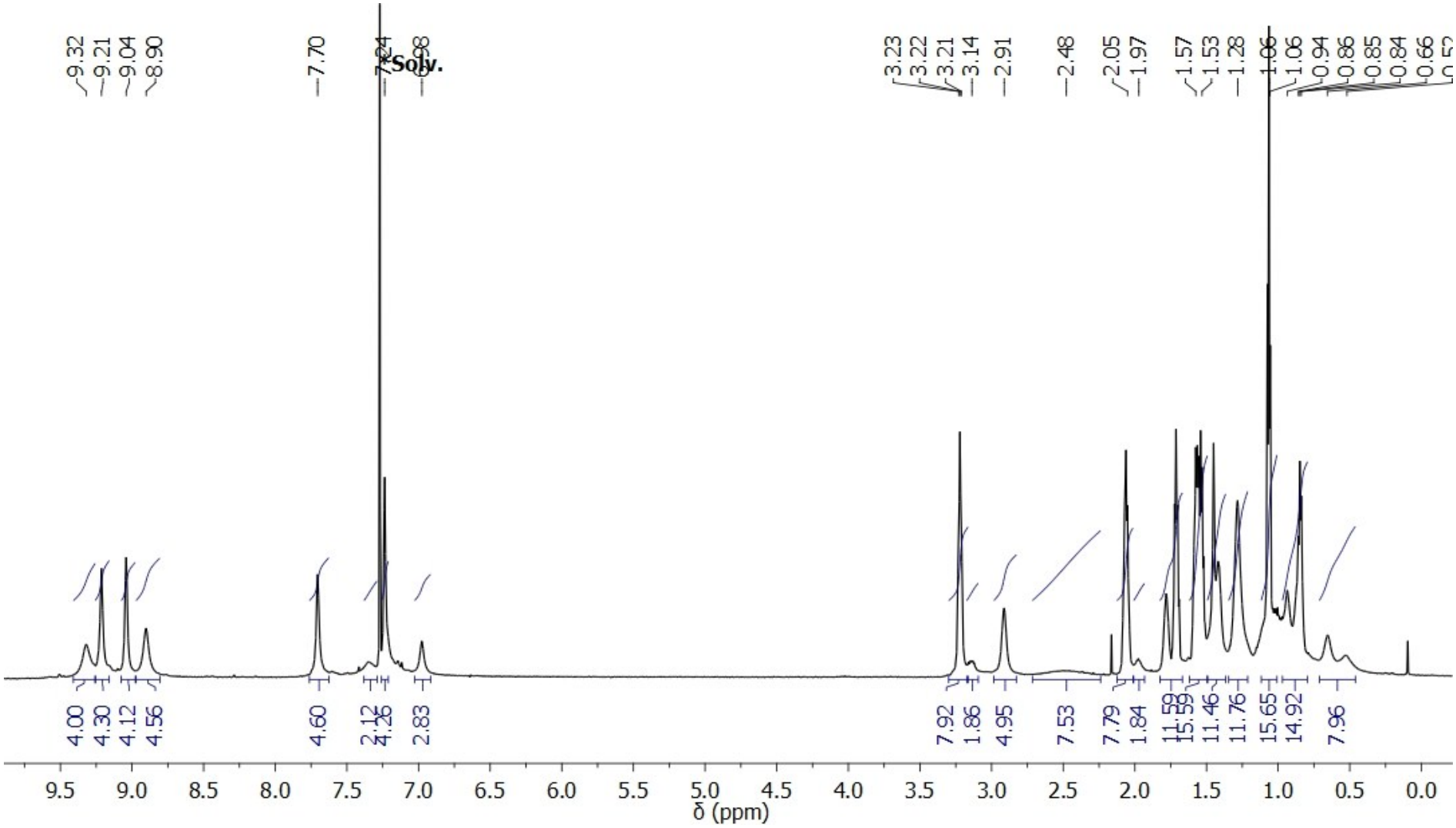

Figure S6. ^{1}H NMR spectrum of **2** (700 MHz, $CDCl_3$, 50 °C).

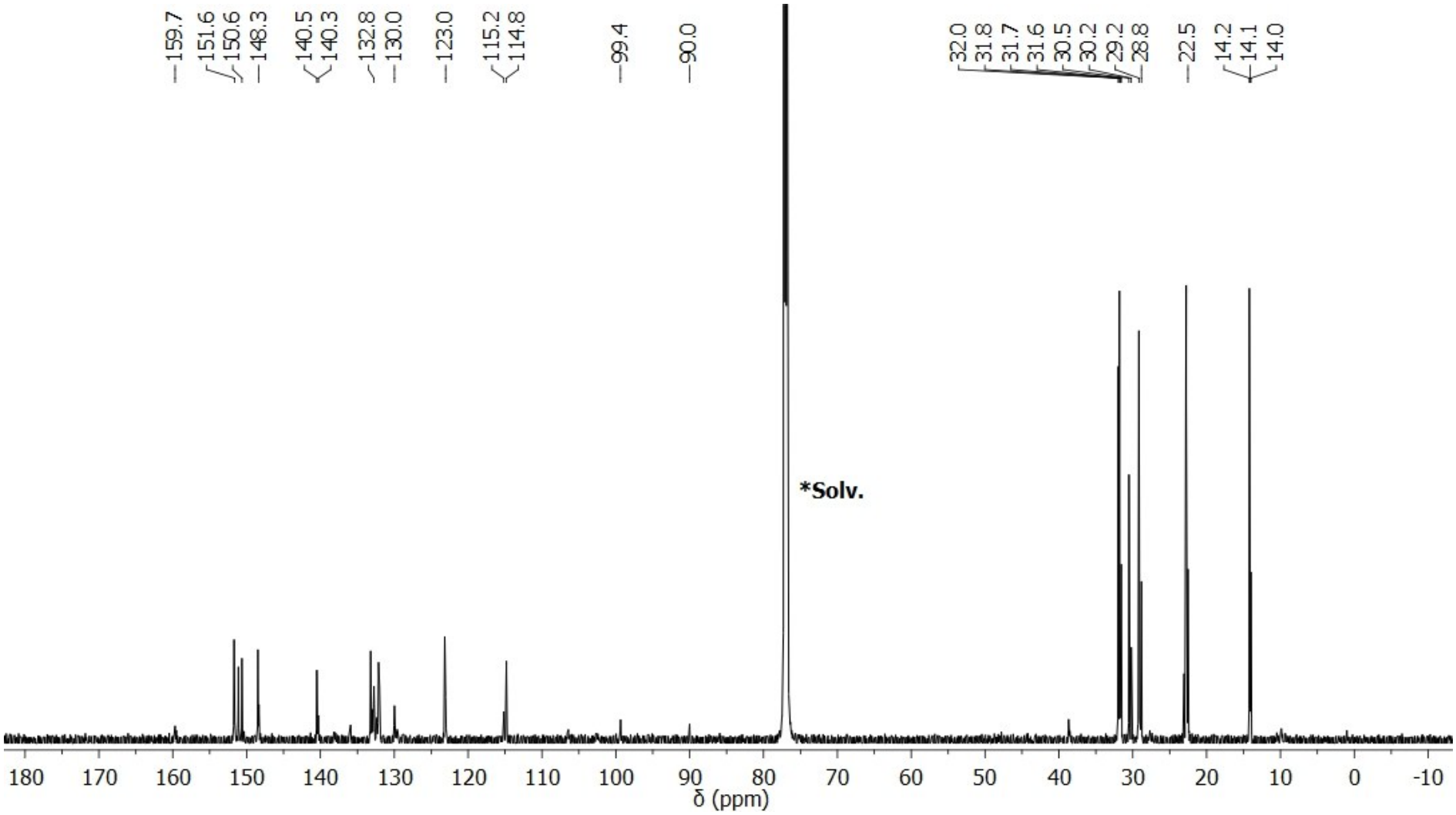

Figure S7. ^{13}C NMR spectrum of **2** (175 MHz, $CDCl_3$, 50 °C).

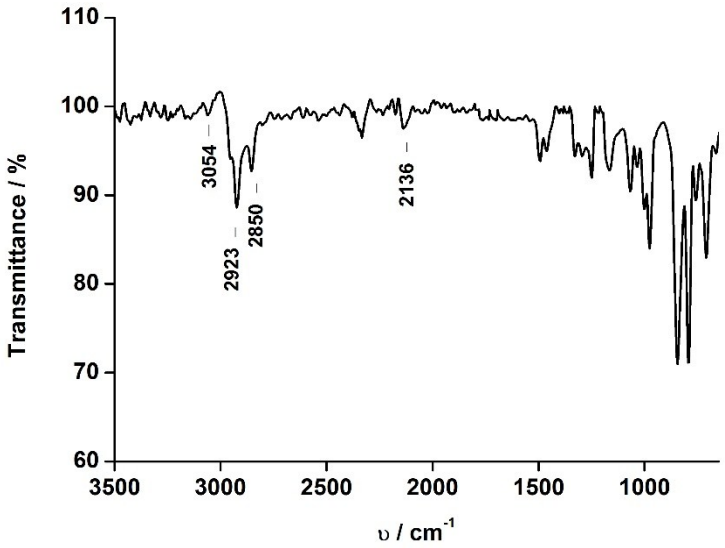

Figure S8. FT-IR spectrum of **6** (ATR).

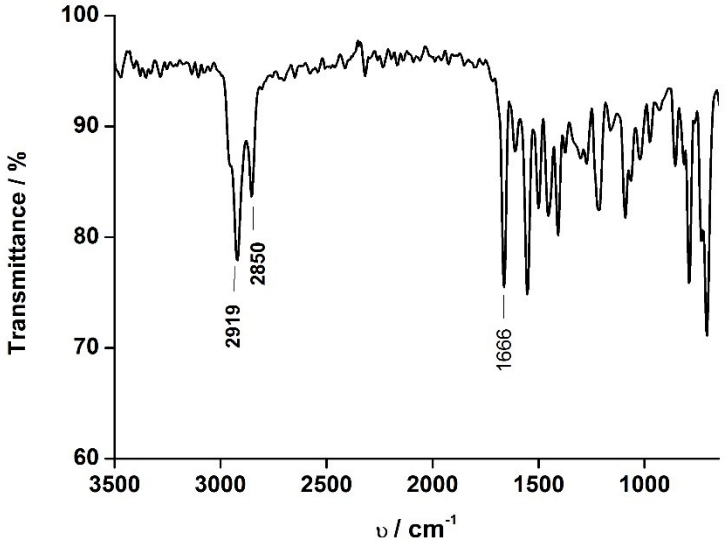

Figure S9. FT-IR spectrum of **1** (ATR).

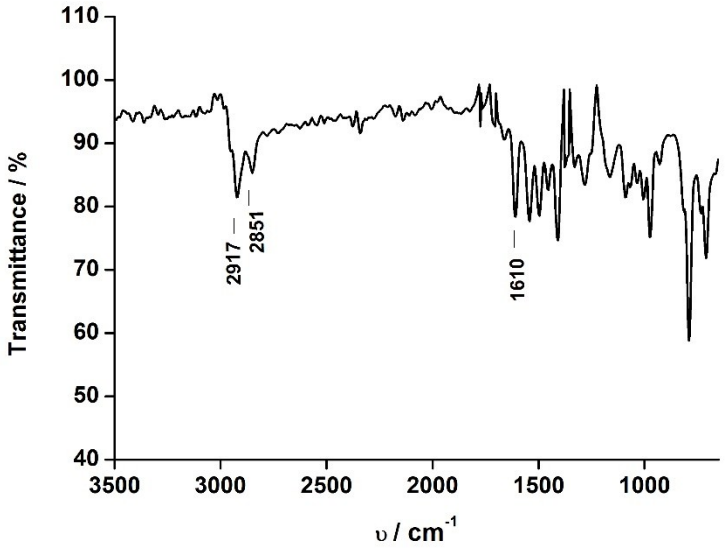

Figure S10. FT-IR spectrum of **2** (ATR).

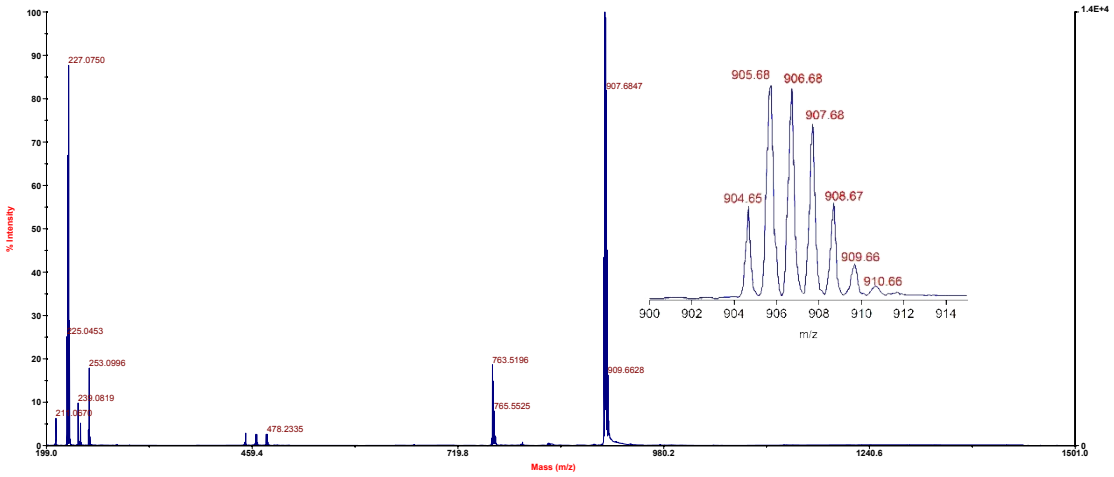

Figure S11. MALDI-TOF MS spectrum of compound $\mathbf{A_3B\text{-}H_2}$.

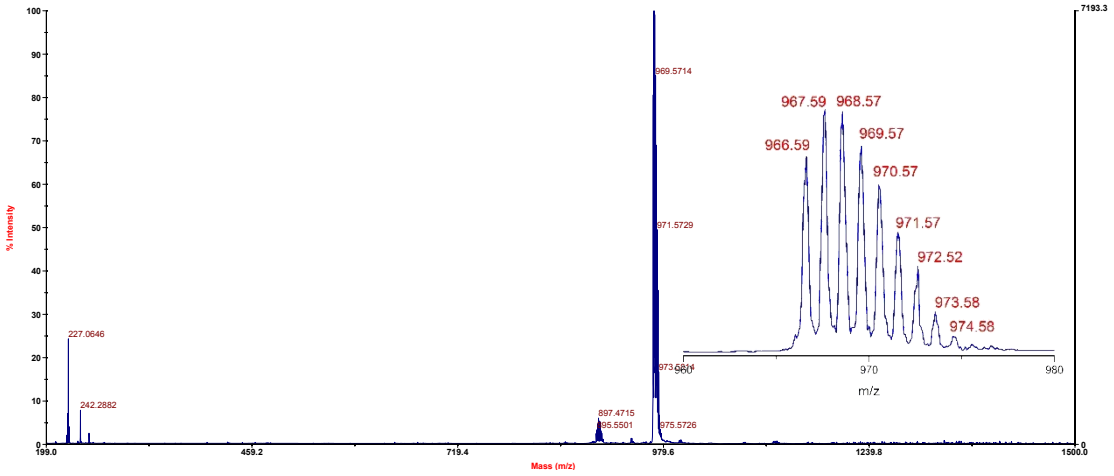

Figure S12. MALDI-TOF MS spectrum of compound **6**.

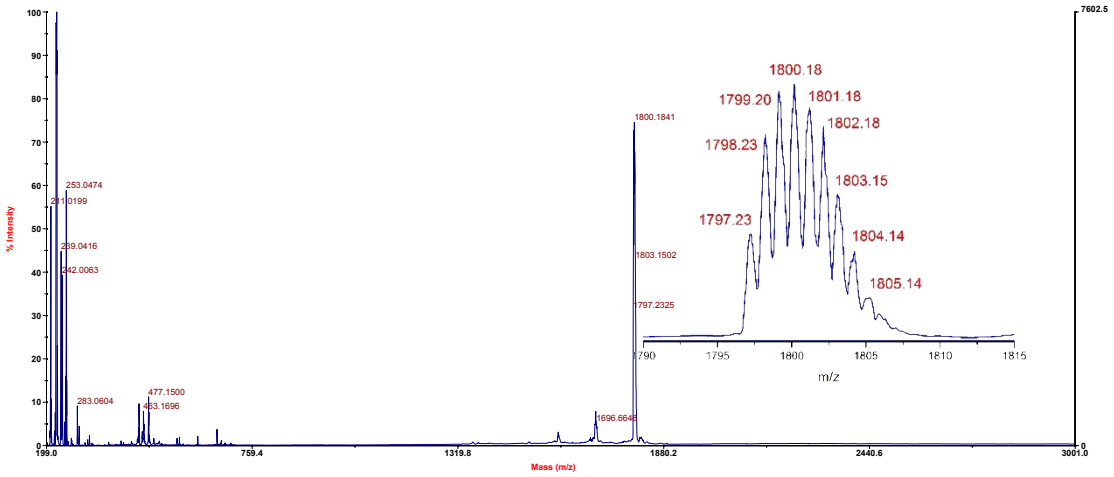

Figure S13. MALDI-TOF MS spectrum of compound **1**.

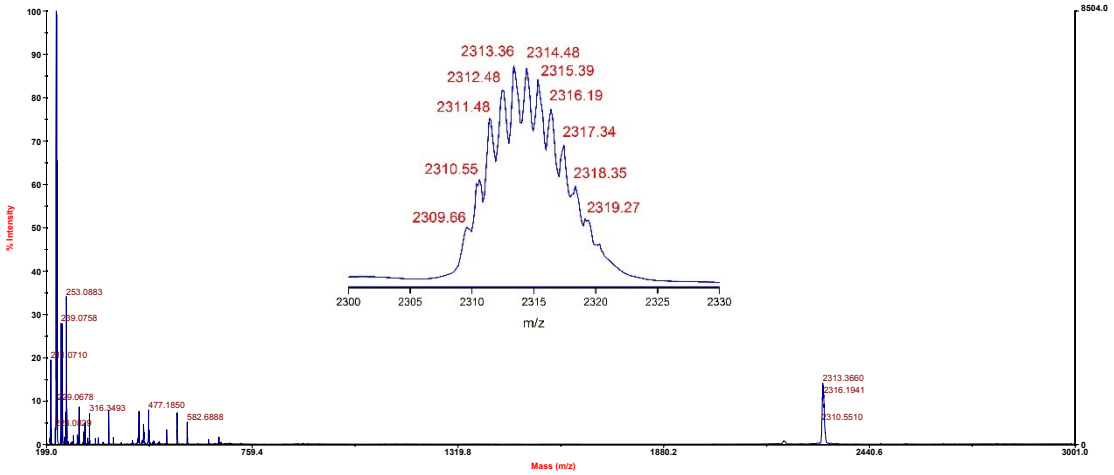

Figure S14. MALDI-TOF MS spectrum of compound **2**.

2. Thermogravimetric analysis of compounds 1 and 2

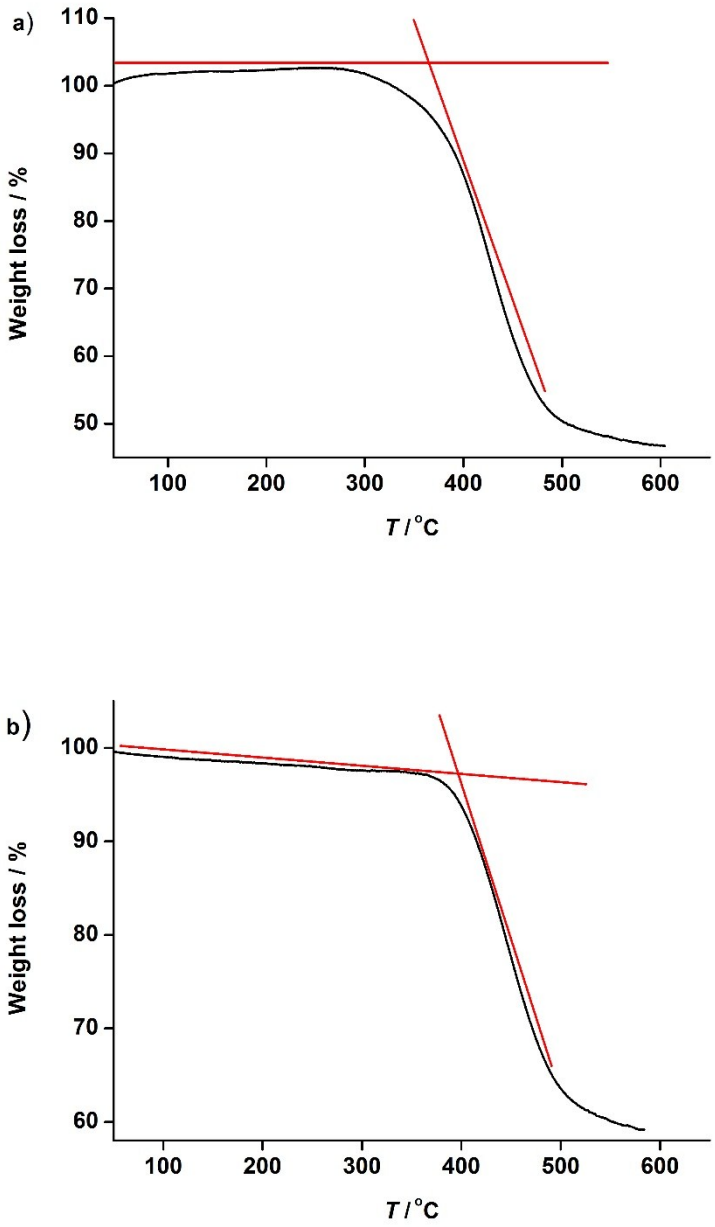

Figure S15. Thermogravimetric analysis of (a) **1** and (b) **2**.

3. Absorption spectra in solutions

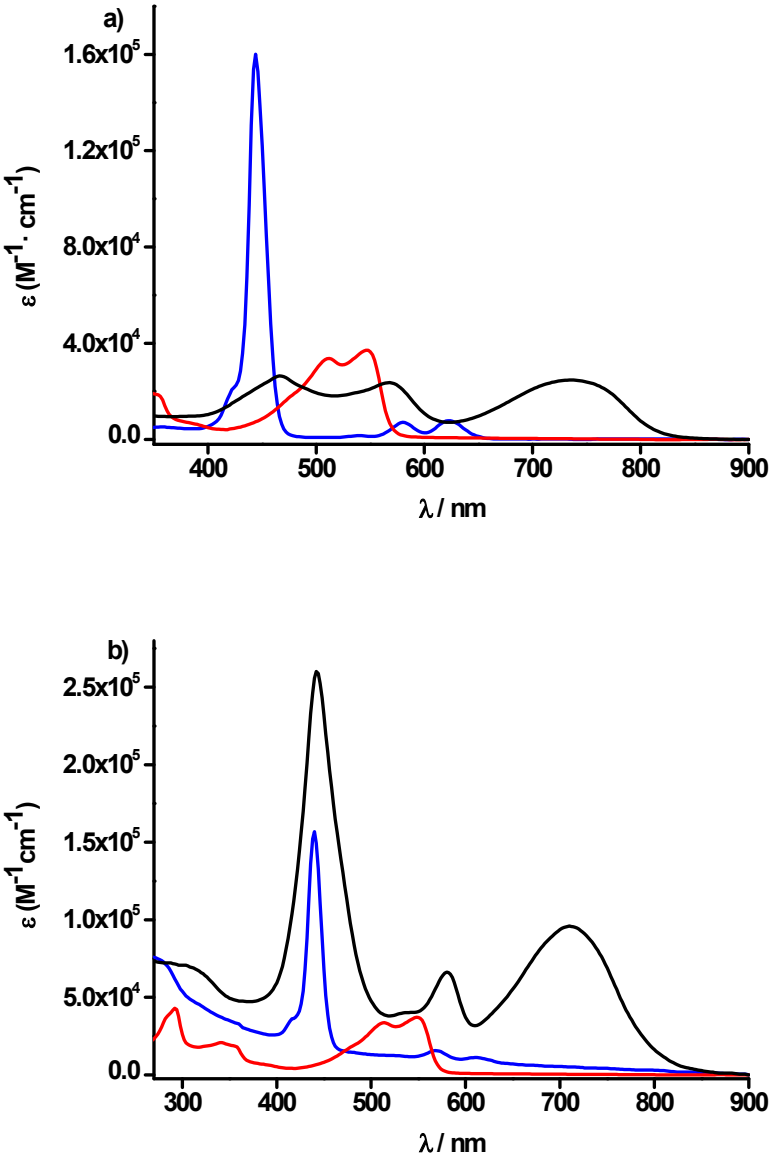

Figure S16. Absorption spectra (CH_2Cl_2, 10^{-6} M) of (a): **3** (—), **DT-DPP** (—) and **1** (—) and (b): **6** (—), **DT-DPP** (—) and **2** (—).

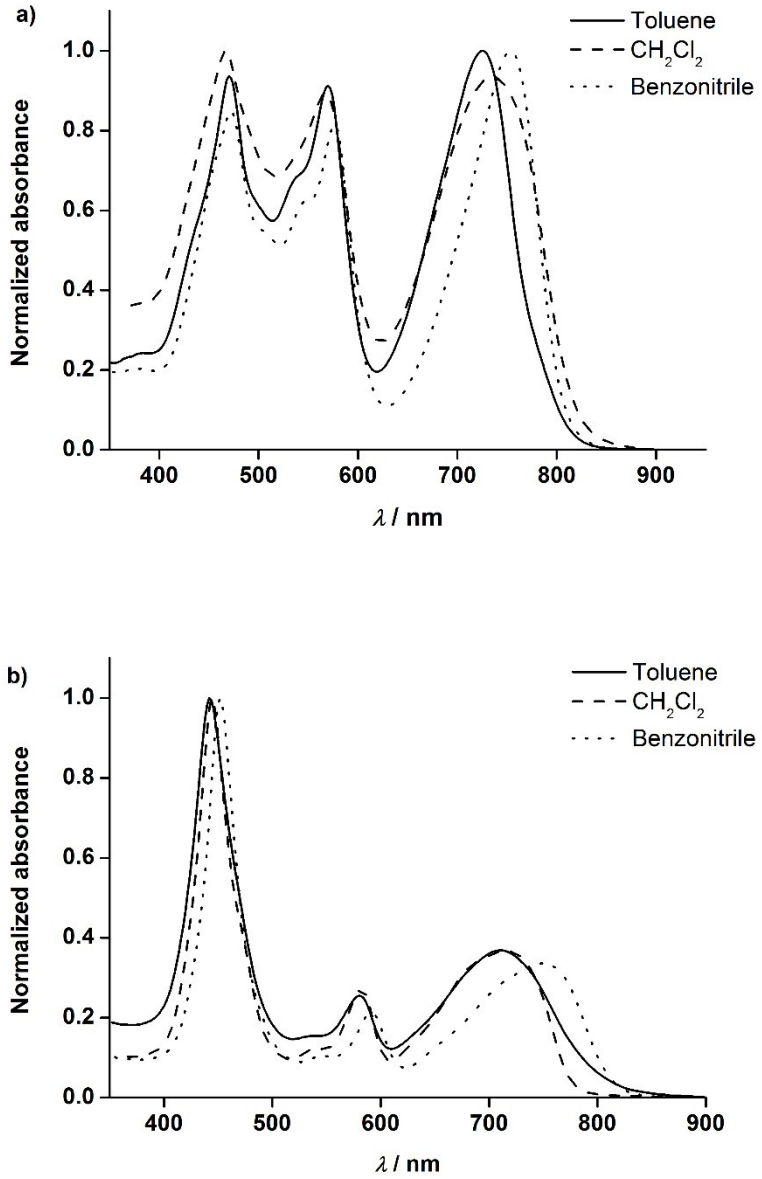

Figure S17. Absorption spectra of (a) **1** and (b) **2** in different solvents (10^{-6} M).

4. Electrochemical studies

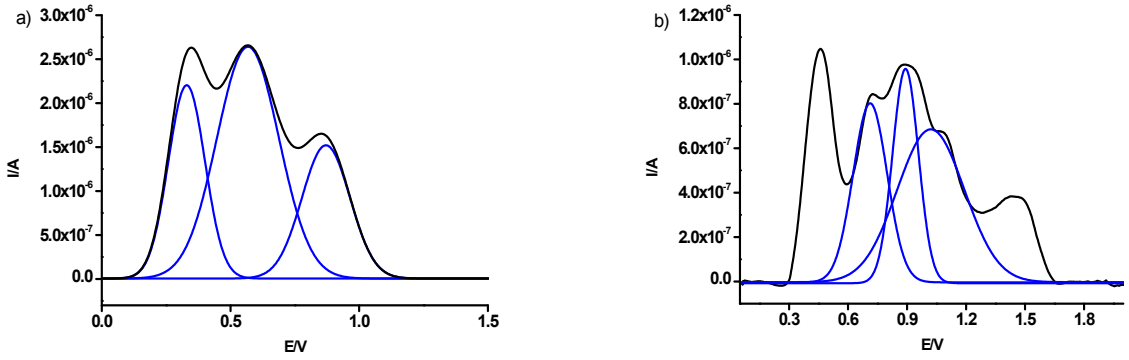

Figure S18. Oxidation OSWV voltammetry a) **1** and b) **2.** Blue: deconvolution of bands.

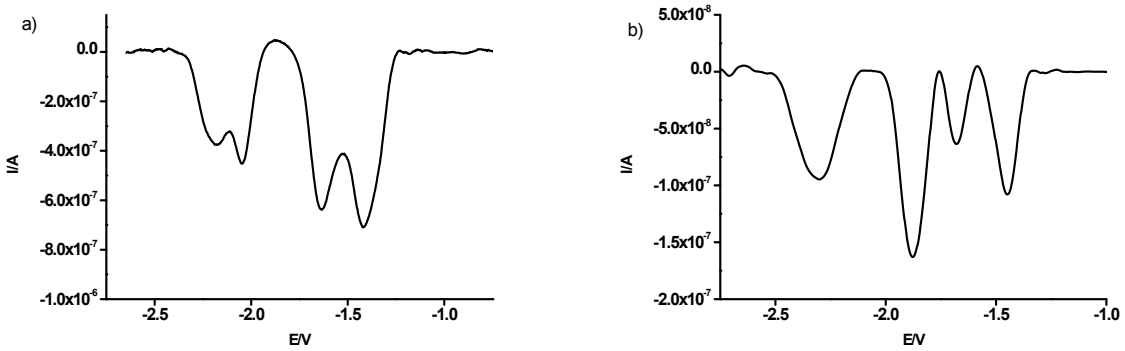

Figure S19. Reduction OSWV voltammetry a) **1** and b) **2.**

5. HOMO and LUMO electron density distribution of 1 and 2

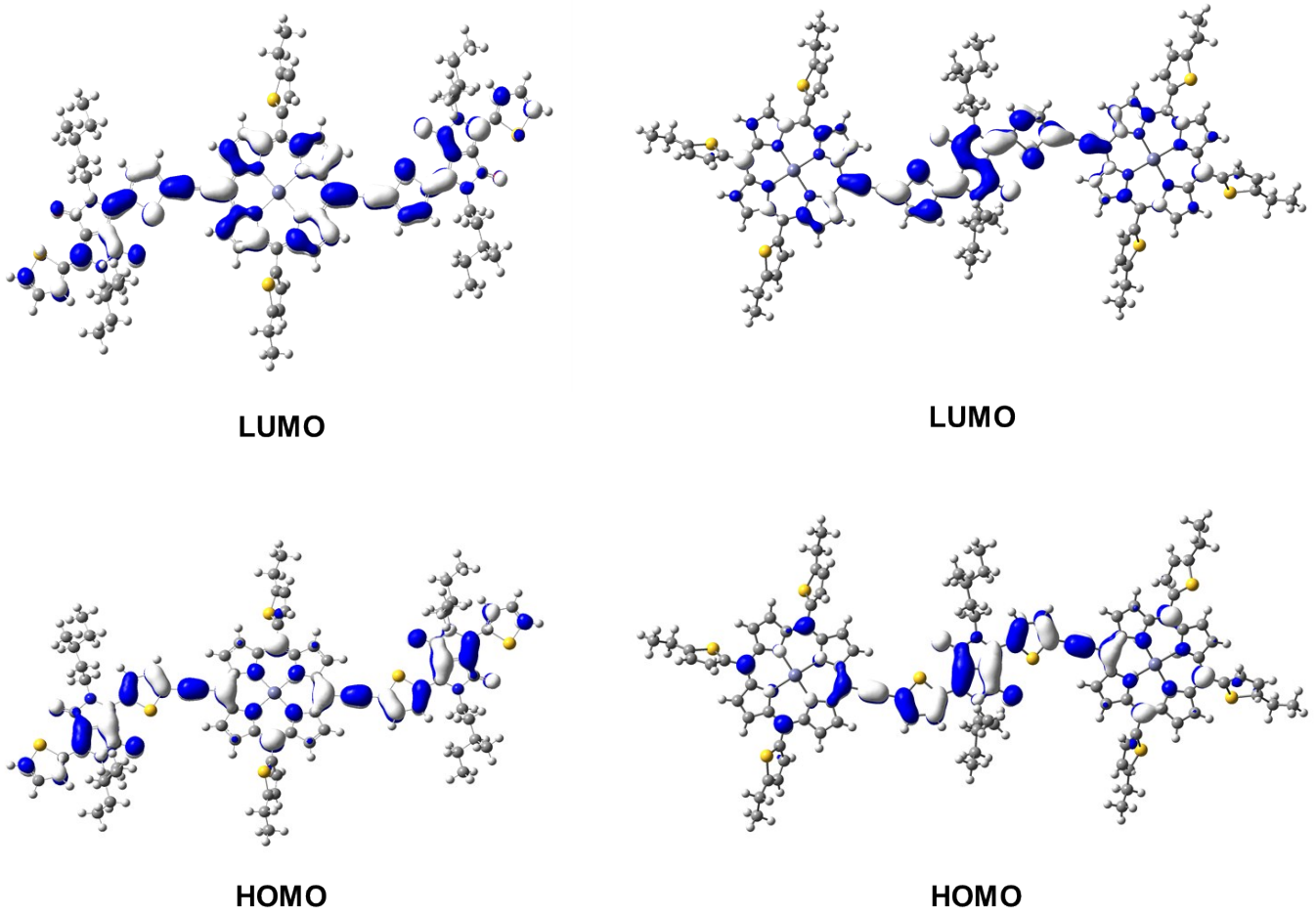

Figure S20. HOMO and LUMO electron density distribution of A–D–A **1** (left) and D–A–D **2** (right). For simplicity in the calculations, hexyl chains are replaced by ethyl.

6. Theoretical optimized geometries of 1 and 2.

a)

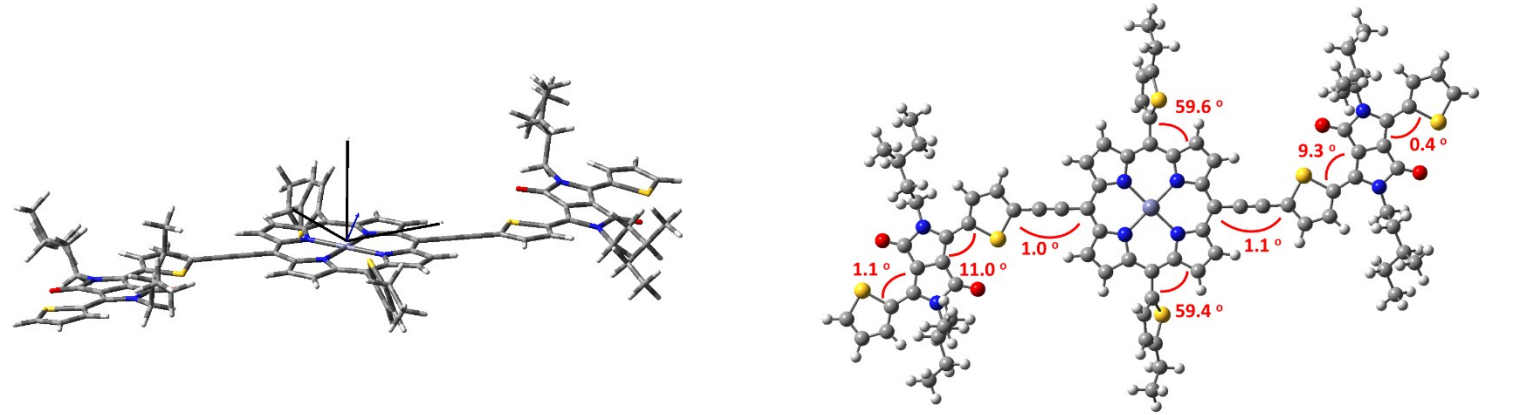

b)

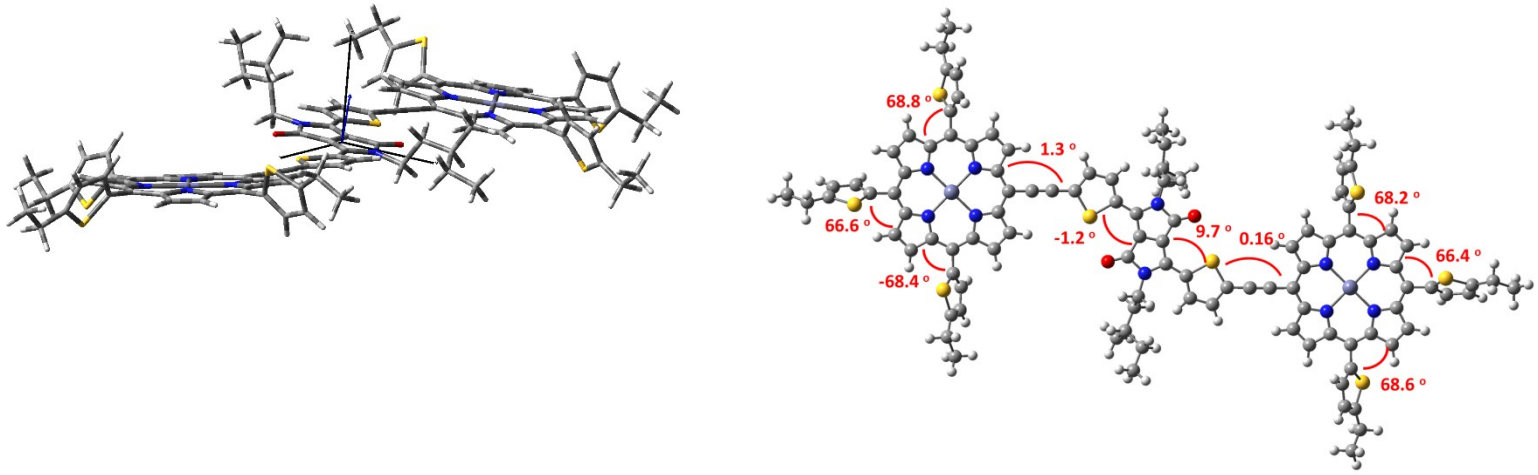

Figure S21. Theoretical optimized geometries and dipole moment of (a) **1** and (b) **2**.

7. Current–voltage plots and IPCE spectra

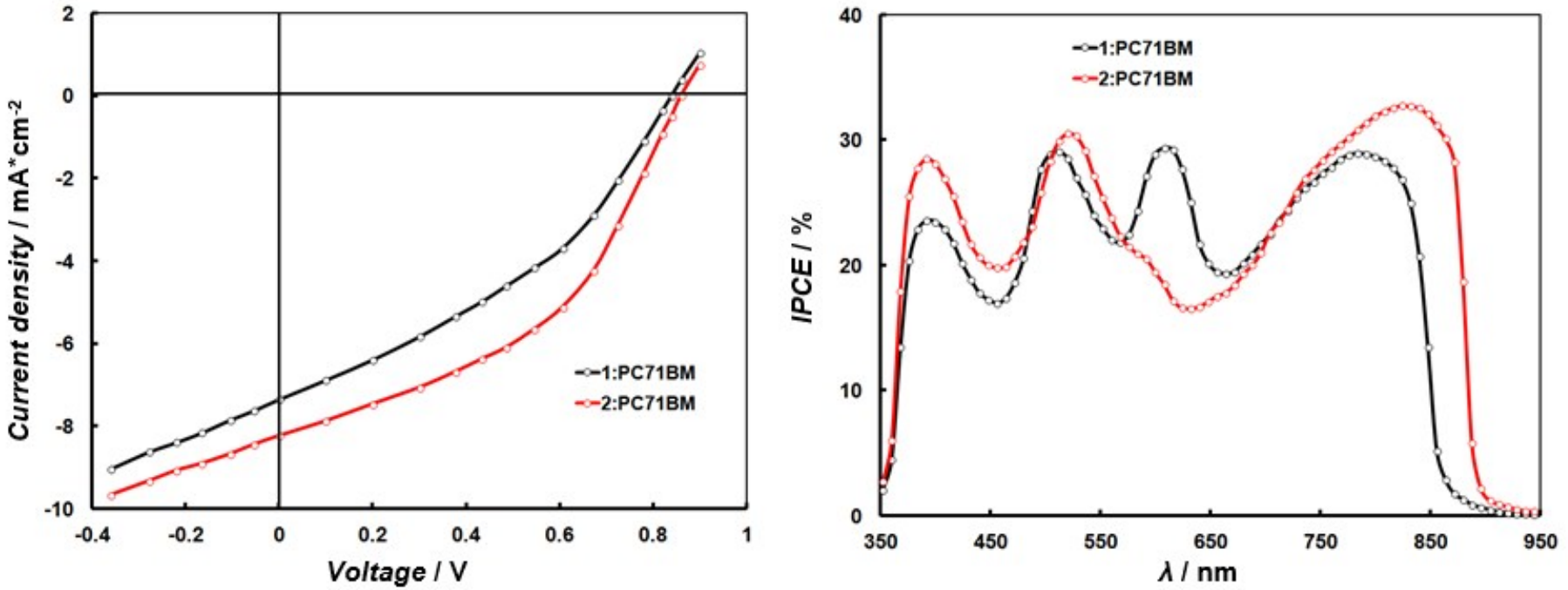

Figure S22. (a) Current –voltage characteristics under illumination and (b) IPCE spectra of the OSCs based on **1**:$PC_{71}BM$ and **2**:$PC_{71}BM$ processed with cholorobenzene solution.